

# Selenium-Doped Cathodes for Lithium–Organosulfur Batteries with Greatly Improved Volumetric Capacity and Coulombic Efficiency

Jinqiu Zhou, Tao Qian,\* Na Xu, Mengfan Wang, Xuyan Ni, Xuejun Liu, Xiaowei Shen, and Chenglin Yan\*

For the first time a new strategy is reported to improve the volumetric capacity and Coulombic efficiency by selenium doping for lithium–organosulfur batteries. Selenium-doped cathodes with four sulfur atoms and one selenium atom (as the doped heteroatom) in the confined structure are designed and synthesized; this structure exhibits greatly improved volumetric/areal capacities, and a Coulombic efficiency of almost 100% for highly stable lithium–organosulfur batteries. The doping of Se significantly enhances the electronic conductivity of battery electrodes by a factor of 6.2 compared to pure sulfur electrodes, and completely restricts the production of long-chain lithium polysulfides. This allows achievement of a high gravimetric capacity of 700 mAh g<sup>-1</sup> close to its theoretical mass capacity, an exceptional volumetric capacity of 2457 mAh cm<sup>-3</sup>, and excellent capacity retention of 92% after 400 cycles. Shuttle effect is efficiently weakened since no long-chain polysulfides are detected from in situ UV/vis results throughout the entire cycling process arising from selenium doping, which is theoretically confirmed by density functional theory calculations.

The development of promising new battery systems using new chemistries and system configurations is being intensified to meet rising standards for long-driving-range, battery-powered electric vehicles, high-performance autonomous aircraft, and robotics. The successful candidates for new generation batteries should achieve many of these performance goals including high capacity and high stability, and may also offer other attractive

attributes, such as being environmentally benign and scalable.<sup>[1]</sup> Lithium–sulfur batteries have been considered one of the most promising candidates since the concept emerged in the 1960s, due to their high specific theoretical energy storage (1675 mAh g<sup>-1</sup>), natural abundance, and low cost of sulfur.<sup>[2,3]</sup> However, several problems hinder their practical application and mass commercialization: 1) the insulating nature of low electronic and ionic conductivity for sulfur, and the insoluble reduction products of low-order sulfides (Li<sub>2</sub>S) lead to low active material utilization; and 2) the high solubility of long-chain lithium polysulfide Li<sub>2</sub>S<sub>x</sub> (4 ≤ x ≤ 8) intermediates in the organic liquid electrolyte. These various soluble polysulfides can freely migrate between the cathode and anode, leading to so-called shuttle effect. The shuttle effect would result in active material loss, uncontrolled dendritic

and mossy lithium growth especially, causing safety issues, low Coulombic efficiency, and poor cycle life.<sup>[4,5]</sup> Many efforts and significant achievements have been made over the last few years to overcome these problems.<sup>[6]</sup>

Organic materials<sup>[7–10]</sup> not only are renowned to be renewable, abundant, sustainable, and environmentally friendly, but also possess promising electrochemical performance with high capacity, molecular controllability, structural diversity, flexibility, the tuning of the redox potential in a wide range, possible multi-electron reactions, and ease in recycling, representing an attractive and emerging paradigm for next-generation energy storage systems. Organosulfur polymer, as a kind of organic materials, was investigated for Li–S batteries. Traditionally, organosulfur polymer was mainly based on thioether compounds, which exhibited relatively low capacity of 100–400 mAh g<sup>-1</sup> and cycling life only for 20–40 cycles.<sup>[11,12]</sup> Recently, sulfur-containing copolymers, by directly using elemental sulfur as a feedstock to copolymerize with poly(acrylonitrile) or 1,3-diisopropenylbenzene, were brought up. However, the length of the sulfur chain in the copolymer could not be controlled, so the long-chain polysulfides generated during cycling would still cause severe shuttle effect; unfavorable for the Coulombic efficiency and reversibility.<sup>[13,14]</sup> Moreover, it remains a challenge to improve the poor kinetics of organosulfur polymers due to the intrinsic low electronic

J. Zhou, Dr. T. Qian, N. Xu, M. Wang, X. Ni, X. Liu, X. Shen, Prof. C. Yan  
Soochow Institute for Energy and Materials Innovations  
College of Physics  
Optoelectronics and Energy & Collaborative Innovation Center  
of Suzhou Nano Science and Technology  
Soochow University  
Suzhou 215006, China  
E-mail: tqian@suda.edu.cn; c.yan@suda.edu.cn

J. Zhou, Dr. T. Qian, N. Xu, M. Wang, X. Ni, X. Liu, X. Shen, Prof. C. Yan  
Key Laboratory of Advanced Carbon Materials and Wearable Energy  
Technologies of Jiangsu Province  
Soochow University  
Suzhou 215006, China

 The ORCID identification number(s) for the author(s) of this article can be found under <https://doi.org/10.1002/adma.201701294>.

DOI: 10.1002/adma.201701294

conductivity of sulfur ( $5 \times 10^{-28} \text{ S m}^{-1}$ ) and the crosslinks between chains.<sup>[4,15]</sup> On the other hand, in addition to gravimetric capacities ( $\text{mAh g}^{-1}$ ), other important metrics such as volumetric ( $\text{mAh cm}^{-3}$ ) and areal ( $\text{mAh cm}^{-2}$ ) capacities should be emphasized. This is because the volumetric capacities can be more important than gravimetric capacities in many practical applications, which required batteries to not only be light in weight but also compact in size.<sup>[16]</sup> Most studies have focused only on the gravimetric capacities, while overlooking the volumetric and areal capacities. As a result, urgent attention should be paid to the development of high-density electrode materials with high volumetric/areal capacities, and a high Coulombic efficiency.

Compared to sulfur, selenium, as a d-electron-containing member of group VIA in the periodic table and a congener of sulfur, has a much higher electronic conductivity ( $1 \times 10^{-3} \text{ S m}^{-1}$ ) and comparable theoretical volumetric capacity ( $3240 \text{ mAh cm}^{-3}$ ), which are important factors for devices where space is limited. However, the theoretical capacity ( $675 \text{ mAh g}^{-1}$ ) of selenium is much lower than that of sulfur, and the selenium cathodes also suffer from cycling deterioration and low Coulombic efficiency owing to the shuttle issue of high-order polyselenide intermediates, similar to sulfur cathodes.<sup>[17–19]</sup> Based on the above complementary features between selenium and sulfur cathodes, selenium-doped sulfur molecules are attractive candidates in lithium–sulfur batteries with superior performance. To our knowledge, many inorganic selenium/carbon<sup>[17,18]</sup> or  $\text{S}_x\text{Se}_y/\text{carbon}$ <sup>[3,19]</sup> composites were widely investigated, but no research about selenium-doped organosulfur polymers has been reported.

Herein, to improve the volumetric capacity and Coulombic efficiency, selenium-doped poly(diallyl tetrasulfide) (PDATtSSe)

with four sulfur atoms and one selenium atom (as the doped heteroatom) in the confined structure is used as cathode material in lithium–organosulfur batteries. The Se doping could enhance the electronic conductivity, improve the Li-ion transport, and the unique molecular structure could suppress the shuttle effect, leading to a gravimetric capacity of  $700 \text{ mAh g}^{-1}$ , close to its theoretical mass capacity, with a high capacity retention of 92% after 400 cycles, and a Coulombic efficiency of almost 100%. Its dense electrode structure, and high electronic and ionic conductivity also permit a high areal loading, delivering a striking volumetric capacity of  $2457 \text{ mAh cm}^{-3}$ , and a high areal capacity of  $5.0 \text{ mAh cm}^{-2}$  for the electrode with an active material loading density up to  $7.07 \text{ mg cm}^{-2}$ , which are crucial parameters for the practical application of lithium–sulfur batteries. The stabilizing mechanism of PDATtSSe cathodes was extensively investigated by density functional theory (DFT) calculations and in situ UV/vis spectroscopy, revealing that the generation of long-chain polysulfides was completely prohibited due to the Se doping. This novel reaction mechanism, along with the improvement in the molecular structure with Se doping, contributed greatly to the improved volumetric capacity and Coulombic efficiency.

We started with the DFT calculations to unveil the potential of PDATtSSe for use as lithium–organosulfur cathodes. The synthetic mechanism of selenium-doped PDATtSSe polymer is demonstrated in **Figure 1A**, with diallyl sulfide (DADS) as precursor and  $\text{SeS}_2$  powders as doping source to realize selenium-doped cathodes.<sup>[20,21]</sup> Changes in the Gibbs free energy were computed and compared to study the bond breaking in the PDATtSSe. As elaborated in Figure S1 (Supporting Information), the homolytic cleavage of the S–Se and S–S bond

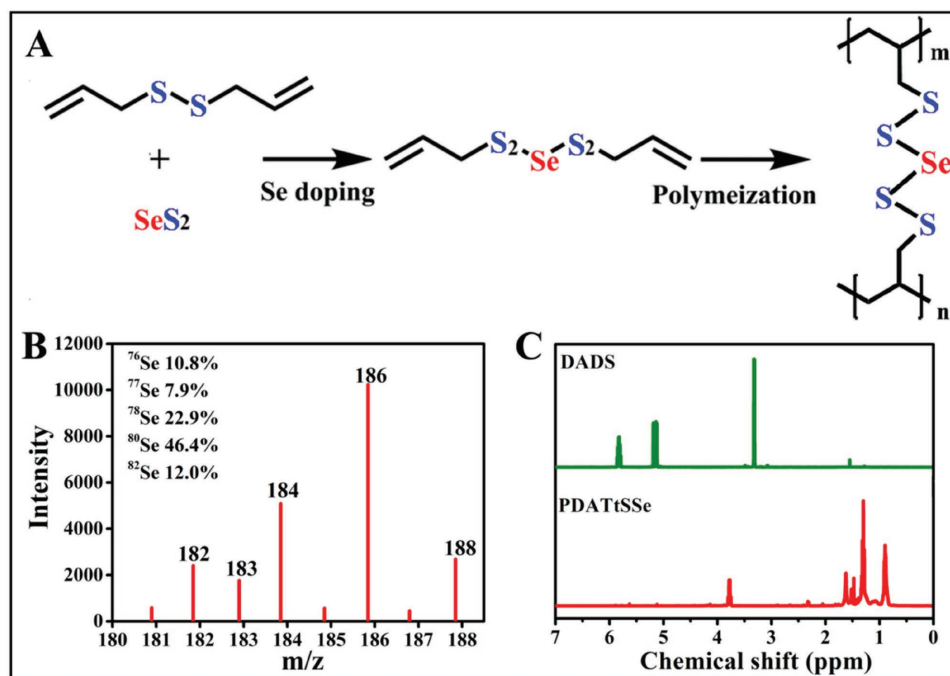


**Figure 1.** A) The synthetic mechanism of selenium-doped PDATtSSe polymer as cathodes for lithium–organosulfur batteries, where  $m$  and  $n$  indicate the degree of polymerization. B) The presence of molecule  $\text{CH}_2=\text{CHCH}_2\text{SSeH}$  ( $m/z = 182, 183, 184, 186,$  and  $188$ ) was confirmed according to the abundance of Se isotopes. C)  $^1\text{H}$  NMR full spectra of the DADS monomer (green line) and PDATtSSe polymer (red line).

delivered dissociation energies of  $-93.02$  and  $-80.94$  kcal mol $^{-1}$ , respectively. These results indicate that the cleavage of the S–Se bond most likely occurs when discharging. With an abundant insertion of Li $^{+}$ , RSLi, Li $_2$ SSe, insoluble Li $_2$ Se, and Li $_2$ S were produced for the next S–S homolytic cleavage of RS $_2$ SeLi and RSSLi, where *R* corresponds to the polymeric carbon chains. In addition, the detailed hypothetical illustration of paths for the cleavage of S–Se and S–S bonds was clearly presented in Figure S2, Supporting Information. This provides conclusive evidence that it is not possible to generate the long-chain soluble polysulfides, which is highly beneficial to the electrochemical performance of lithium–sulfur cathodes.

To give more powerful and convincing evidence for the incorporation of SeS $_2$  into DADS molecule prior to polymerization, the mass spectrometry measurement for the DADS with SeS $_2$  (DATtSSe) was conducted. As shown in Figure 1B, the presence of molecule CH $_2$ =CHCH $_2$ SSeH ( $m/z$  = 182, 183, 184, 186, and 188) is confirmed according to the abundance of Se isotopes. The calculated abundance of isotopic ratio for element Se is displayed in the inset of Figure 1B ( $^{76}\text{Se}$  10.8%,  $^{77}\text{Se}$  7.9%,  $^{78}\text{Se}$  22.9%,  $^{80}\text{Se}$  46.4%, and  $^{82}\text{Se}$  12%),<sup>[22]</sup> consistent with the natural abundance of Se isotopes. The CH $_2$ =CHCH $_2$ SSeH is derived from the DATtSSe due to the dissociation of S–Se bond because the molecule DATtSSe is not stable at the high vaporization temperature. The detection of CH $_2$ =CHCH $_2$ SSeH can convincingly validate the SeS $_2$  has been successfully integrated into the DADS molecule through covalent bonding prior to its polymerization.

To certify the occurrence of the polymerization reaction, Fourier transform infrared spectroscopic analysis was conducted to identify changes in the interactions within the DADS monomer and PDATtSSe polymer in the range of 4000–400 cm $^{-1}$  (Figure S3, Supporting Information). The presence of stretching (3085 cm $^{-1}$ ) and out-of-plane bending

vibrations (990 and 910 cm $^{-1}$ ) of the C–H group, and the stretching vibration of C=C (1635 cm $^{-1}$ ) arising from the allyl groups are consistent with the molecular structure of DADS. After polymerization, these characteristic peaks all disappear, and peaks of the stretching (3000–2800 cm $^{-1}$ ) and bending vibration (1490–1350 cm $^{-1}$ ) of C–H derived from a saturated hydrocarbon radical are enhanced, which provides evidence for the successful polymerization reaction. Furthermore,  $^1\text{H}$  NMR characterization was carried out (Figure 1C). After polymerization, the allyl proton resonances at  $\delta$  = 5.84 and 5.12 ppm associated with the DADS monomer disappear, which further verifies the occurrence of the polymerization reaction.

We next assessed the electrochemical performance of the PDATtSSe polymer as a cathode material by pairing it with metallic Li foils. The areal loading density of active materials is  $\approx 1.4$  mg cm $^{-2}$  for this part of the evaluation. The Coulombic efficiency is a crucial property for lithium–sulfur batteries. Ordinary lithium–sulfur batteries in ether-based electrolytes without lithium nitrate (LiNO $_3$ ) additive may suffer from the “shuttle” effect, resulting in a poor Coulombic efficiency and lithium dendrite growth.<sup>[23]</sup> Excellent Coulombic efficiency could be obtained by selenium doping in lithium–organosulfur battery due to the effectively suppressed shuttle effect. Here, the Coulombic efficiencies for PDATtSSe cathodes using an electrolyte with and without LiNO $_3$ , poly(diallyl pentasulfide) (PDAPtS, five sulfur atoms in the molecular structure), and sulfur cathodes using LiNO $_3$ -free electrolyte were tested (Figure 2A). Coulombic efficiency of over 98% could be achieved for Li/PDATtSSe cell in an electrolyte without LiNO $_3$  compared to the electrolyte with LiNO $_3$  of about 100%. However, relatively low values of 91% for the PDAPtS cathode, and 85% for the sulfur cathode, reveal that the shuttle effect for the PDATtSSe cathode was greatly weakened as no long-chain lithium polysulfides and polyselenides

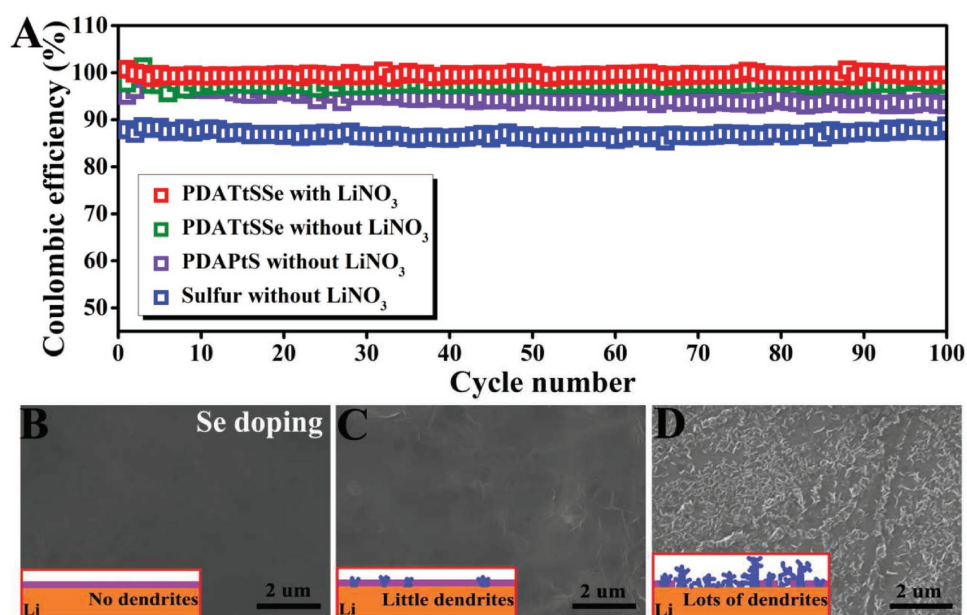


**Figure 2.** A) The Coulombic efficiencies of the PDATtSSe cathodes using an electrolyte with and without LiNO $_3$ , and PDAPtS and sulfur cathodes using a LiNO $_3$ -free electrolyte. B–D) SEM images of the lithium anode surface of PDATtSSe, PDAPtS, and pure sulfur cathodes at a current density of 600 mA g $^{-1}$  operated in an electrolyte without LiNO $_3$  after 100 cycles, respectively.

were generated in the Li/PDATtSse battery during discharging and charging. The superficial morphologies observed by scanning electron microscopy (SEM) and energy dispersive X-ray spectroscopy measurements of the lithium foil anodes for the Li/PDATtSse, Li/PDAPtS, and Li/sulfur cells after 100 cycles in the LiNO<sub>3</sub>-free electrolyte were also investigated. As a common sense, the solid electrolyte interface (SEI) layer is formed due to the reaction of Li metal with solvents and lithium salts<sup>[24]</sup> with products of LiF, Li<sub>2</sub>S<sub>2</sub>O<sub>3</sub>, Li<sub>2</sub>CO<sub>3</sub>, and Li<sub>3</sub>N.<sup>[25]</sup> For Li/PDATtSse, a smooth morphology and a very dense and uniform SEI layer on the top surface of the lithium foil can be observed (Figure 2B). In addition, the least amount (4.18 wt%) of element S mainly derived from the SEI layer was detected on the Li anode surface (Figure S5A,D, Supporting Information) and no signal of element Se was observed (Figure S5A, Supporting Information), confirming again that the shuttle effect was greatly suppressed in the Li/PDATtSse cell due to the Se doping. By contrast, the lithium anode of the Li/PDAPtS battery exhibited a slightly rough morphology (Figure 2C) and the amount of element S was 7.8 wt% (Figure S5B,D, Supporting Information), implying the deposition of short-chain Li<sub>2</sub>S<sub>x</sub> on Li surface. However, uneven deposition short-chain Li<sub>2</sub>S<sub>x</sub> as well as irregular and blade-like lithium dendrites on the Li anode were clearly observed when sulfur cathode was used<sup>[26]</sup> (Figure 2D), leading to dead lithium and performance deterioration. Moreover, the largest amount (19.44 wt%) of element S (Figure S5C,D, Supporting Information) was detected on the Li surface, resulted from the severe short-chain Li<sub>2</sub>S<sub>x</sub> deposition due to shuttle effect. Furthermore, the morphology changes of PDATtSse and sulfur cathodes before and after cycling were

also observed through SEM<sup>[5]</sup> (Figure S6, Supporting Information). Apparently, the morphology of the PDATtSse cathodes was still maintained and no obvious change could be observed after cycling. While for sulfur cathode, large and nonuniform polysulfides after cycling were observed on the cathode surface, which provided powerful evidence that the shuttle effect was greatly weakened in the Li/PDATtSse cell due to the Se doping.

Figure 3A depicts the cyclic voltammetry (CV) curves of the PDATtSse polymer scanned at 0.01 mV s<sup>-1</sup> during the second cycle. Due to the reduction of the S–S and S–Se bonds, two small cathodic waves at ≈2.25 and ≈2.12 V can be seen in the negative sweep, followed by a large cathodic peak with an onset potential of 2.07 V, a peak centered at 1.98 V, as well as a small wave at 1.75 V.<sup>[4,19]</sup> During the following anodic scan, the peak at 2.3 V was attributed to the deintercalation of lithium ions. No obvious changes in the CV peak positions or peak current were observed in the subsequent curves (Figure S7A, Supporting Information),<sup>[27]</sup> which confirms the electrochemical stability of PDATtSse.

These are consistent with the galvanostatic charge/discharge profiles of the second cycle at a current density of 200 mA g<sup>-1</sup> based on mass of PDATtSse (Figure 3B). Moreover, the PDATtSse cathode delivered a discharge capacity of 700 mAh g<sup>-1</sup>, which is close to its theoretical capacity of 742 mAh g<sup>-1</sup>, of which 650 mAh g<sup>-1</sup> can be recovered and reversibly sustained afterward (Figure S7B, Supporting Information). The stability during extended cycling can be broadened to 400 cycles by employing a current density of 600 mA g<sup>-1</sup> based on mass of PDATtSse, with a simultaneous exceptional capacity retention of 92%, a reversible capacity of 500 mAh g<sup>-1</sup>, and a high Coulombic efficiency of ≈100%

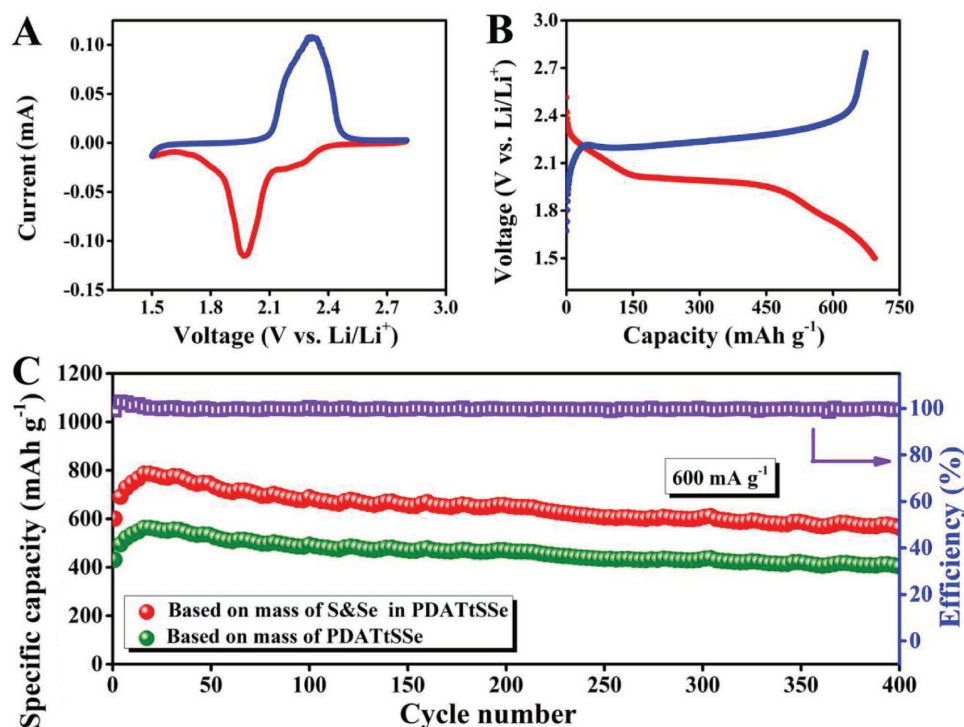


**Figure 3.** A) The CV profiles of the second cycle at a scan rate of 0.01 mV s<sup>-1</sup>. B) Voltage profiles of the second cycle at a current density of 200 mA g<sup>-1</sup> for the PDATtSse cathode. C) The stability during extended cycling and Coulombic efficiency of the PDATtSse for 400 cycles at a current density of 600 mA g<sup>-1</sup> based on mass of PDATtSse and mass of S and Se in PDATtSse, respectively.

(Figure 3C). This corresponds to a small average capacity loss of 0.02% per cycle, attesting to its outstanding long-term cycling performance. The corresponding galvanostatic charge–discharge voltage profiles are displayed in Figure S8A (Supporting Information), revealing negligible changes in both the shape and specific capacity during 100 cycles. The content of S and Se in the PDATtSSe is calculated to be 71.6 wt%. The specific capacities based on the mass of PDATtSSe and the mass of S and Se in the PDATtSSe were both shown in Figure 3C. For comparison, the cycling performance of PDAPtS cathode without Se doping was also demonstrated (Figure S8B, Supporting Information). A poor capacity retention of  $\approx 50\%$  was obtained since it was easier to generate polysulfides during the cycling process. In Figure S8C (Supporting Information), it can be observed that the PDATtSSe presents an impressive rate capacity, even at a maximum current density of  $1200 \text{ mA g}^{-1}$ . When the specific current ramped up stepwise from 50 to 100, 200, 500, 800, 1000, and  $1200 \text{ mA g}^{-1}$ , specific capacities of 740, 632, 570, 490, 422, 373, and  $333 \text{ mAh g}^{-1}$  were reversibly

obtained, respectively. The corresponding galvanostatic charge–discharge voltage profiles are displayed in Figure S8D (Supporting Information). As the current rate is increased, the plateaus are shortened and decline due to the electrode polarization, in agreement with previous reports.<sup>[28]</sup> Then, the current density abruptly returns to  $200 \text{ mA g}^{-1}$ , with a capacity of  $555 \text{ mAh g}^{-1}$  that was reversibly measured. The outstanding kinetic behavior should be closely associated with the improved electronic transport and lithium-ion diffusion characteristics of the PDATtSSe, which could be further supported by their relatively lower charge transfer resistances ( $R_{CT}$ ) and faster lithium-ion diffusion coefficient ( $D_{\text{Li}^+}$ ) compared with that of PDAPtS and sulfur powders discussed below.

Electrochemical impedance spectroscopy (EIS) measurements were carried out to gain further insight into the prominent electrochemical properties, and the equivalent circuit models of the studied systems are shown in the insets of Figure 4A,B to represent the internal resistance of the electrodes. It can be seen that the impedance spectra can be

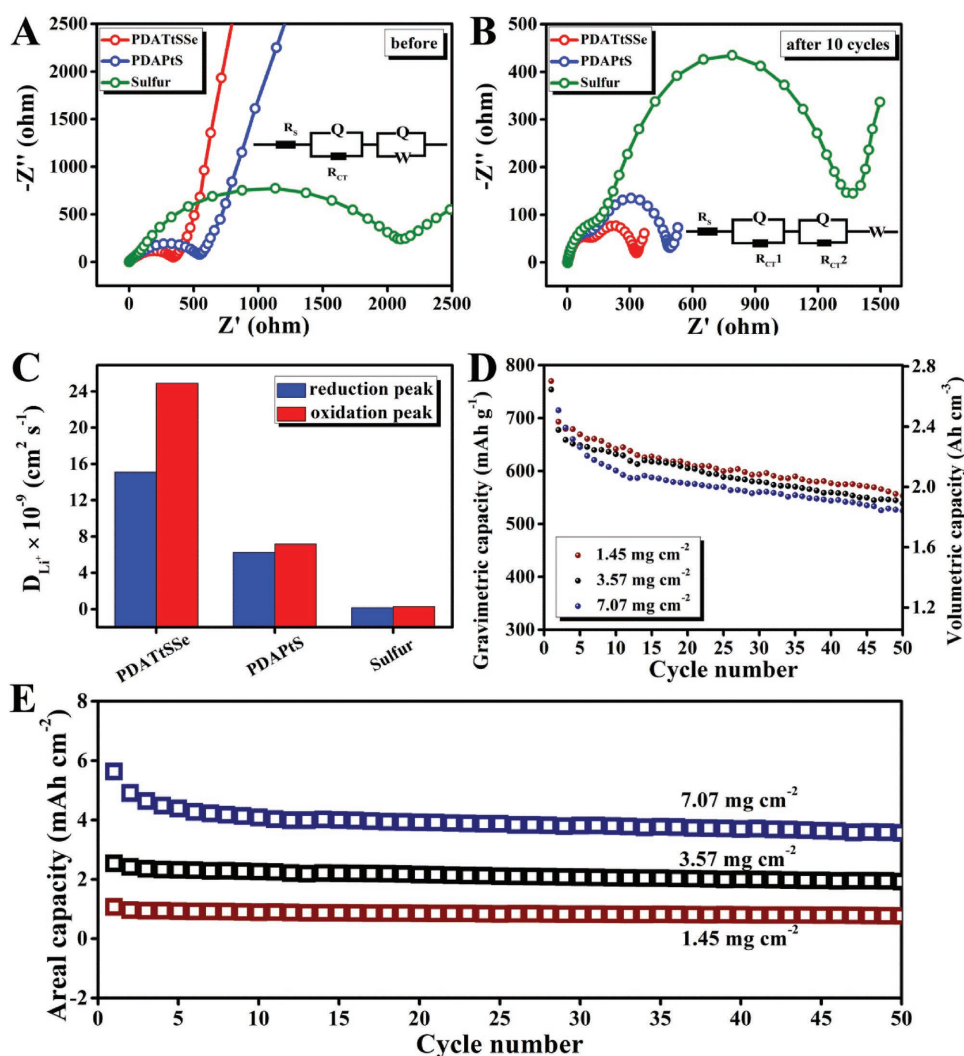


**Figure 4.** Comparison of EIS results of cells with PDATtSSe, PDAPtS, and pure sulfur cathodes A) before and B) after ten cycles. C)  $\text{Li}^+$  diffusion coefficients of the PDATtSSe, PDAPtS, and pure sulfur cathodes. D) Gravimetric and volumetric capacities at a current density of  $200 \text{ mA g}^{-1}$ , and E) areal capacities with different PDATtSSe loadings as indicated. These capacities are all calculated based on the active materials.

divided into two types according to the shape of the curves. One type of impedance curves before cycling (see Figure 4A) is composed of one depressed semicircle in the high frequency (HF) region, while the other type of impedance spectra after ten cycles (see Figure 4B) exhibited two depressed semicircles at both the HF and middle frequency (MF) range. The depressed semicircle in the HF region may reflect the charge transfer process ( $R_{CT}$ ) at the conductive agent interface, and the depressed semicircle in the MF range may be attributed to the formation of insoluble polysulfide species ( $R_{CT2}$ ).<sup>[29]</sup> In addition, the intercepts in the high frequency regions were attributed to the electronic resistance of the cathodes and ionic resistance of the liquid electrolyte ( $R_S$ ).<sup>[30]</sup> The fitted impedance parameters are listed in Table S1 (Supporting Information). Clearly, irrespective of whether before or after cycling, the values of the charge-transfer impedance ( $R_{CT}$ ) of the PDATtSSe battery were the lowest among the three electrodes, which validates that selenium doping can greatly enhance the electron conductivity of PDATtSSe electrode compared to pure sulfur electrode during the electrochemical lithium insertion/extraction reaction.<sup>[19,31]</sup> Moreover, the much smaller MF semicircle observed in the PDATtSSe battery after ten cycles indicates that the lower polarization and more uniform deposition of insoluble polysulfide species<sup>[29]</sup> results in a significant improvement in the electrochemical performance. In addition, from the results of four-point probe measurements (Figure S9, Supporting Information), it can be found that the PDATtSSe electrode ( $0.33 \text{ S cm}^{-1}$ ) is more conductive than the sulfur electrode ( $0.053 \text{ S cm}^{-1}$ ) by a factor of 6.2.

In addition, CV analysis of PDATtSSe, PDAPtS, and pure sulfur batteries (Figure S10, Supporting Information) was conducted to evaluate the  $D_{Li^+}$  using the Randles–Sevcik equation, as described below

$$I_p = 2.69 \times 10^5 n^{1.5} A D_{Li^+}^{0.5} \nu^{0.5} C_{Li^+} \quad (1)$$

where  $I_p$  indicates the peak current (A),  $n$  is the number of electrons in the reaction,  $A$  is the electrode area ( $\text{cm}^2$ ),  $\nu$  is the scan rate ( $\text{V s}^{-1}$ ), and  $C_{Li^+}$  is the lithium-ion concentration in the electrolyte ( $\text{mol cm}^{-3}$ ).<sup>[32]</sup> From the linear relationship of  $I_p$  and  $\nu^{0.5}$  (Figure S10, Supporting Information),  $D_{Li^+}$  of two reduction and oxidation peaks were obtained, as shown in Figure 4C. It is worth noting that  $D_{Li^+}$  for the two redox peaks of the PDATtSSe battery was much higher than the other two battery systems, suggesting that selenium doping also facilitates fast Li-ion transport, which enhances the electrochemical performance for lithium storage in terms of high loadings, which plays a key role in real battery systems.

Despite its appealing gravimetric activity at the relatively low PDATtSSe loading of  $1.4 \text{ mg cm}^{-2}$ , other important battery metrics including volumetric capacity ( $\text{mAh cm}^{-3}$ ) and areal capacity ( $\text{mAh cm}^{-2}$ ) are important in controlling the performance in practical applications, directly correlating with the actual battery size, pack-level energy density, and lower fabrication cost.<sup>[16,33]</sup> As a result, we prepared electrodes with higher PDATtSSe loadings of  $3.57$  and  $7.07 \text{ mg cm}^{-2}$ . The electrodes with three different mass loadings deliver gravimetric capacities between  $677$  and  $714 \text{ mAh g}^{-1}$ , and volumetric capacities

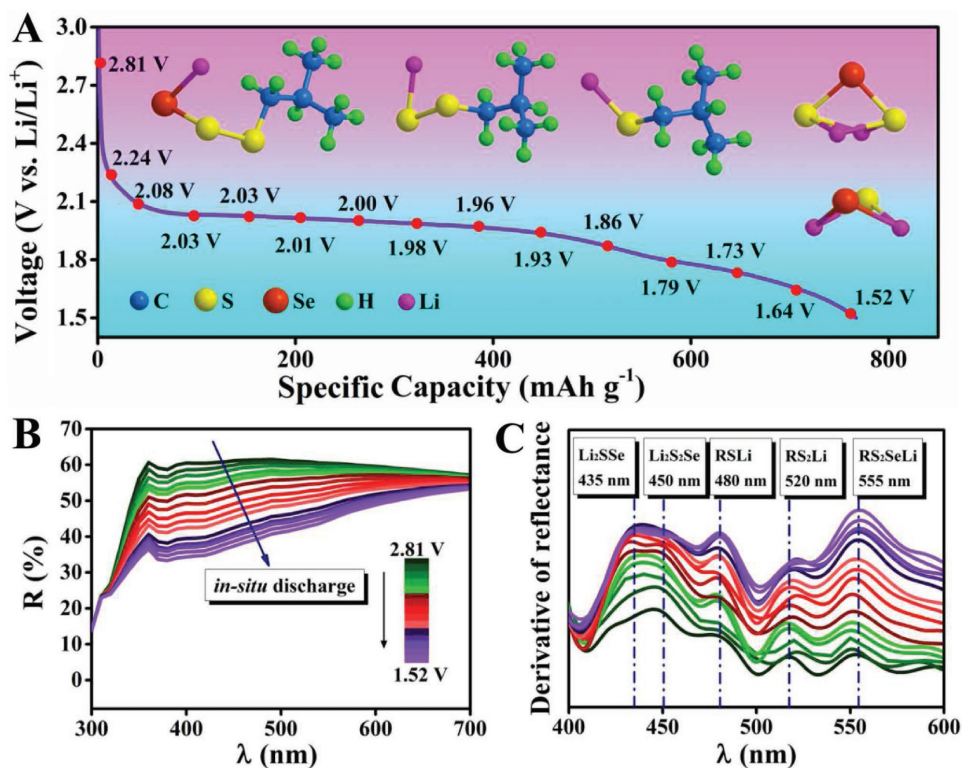


**Figure 5.** A) Discharge profile of the PDATtSSe cell cycled at  $200 \text{ mA g}^{-1}$ , corresponding to the different discharge voltages. B) In situ UV/vis spectra and C) homologous first-order derivatives of the PDATtSSe cell.

between 2376 and 2506 mAh cm<sup>-3</sup> (Figure 4D) are delivered (Tap density of PDATtSSe is 3.51 g cm<sup>-3</sup>). Their areal capacities linearly scale with the areal loading, reaching an outstanding value of 5.0 mAh cm<sup>-2</sup> (Figure 4E).

To further explore the mechanism of the PDATtSSe reduction and the component transformation, in situ UV/vis spectroscopy was carried out at different stages during the discharging process (Figure 5A) by monitoring the changes of the intermediates in the electrolyte. The in situ UV/vis spectra, and the corresponding first-order derivatives of the PDATtSSe electrode, are displayed in Figure 5B,C. No peaks were shifted during the PDATtSSe cell discharge process; hence, no long-chain polysulfide intermediates formed. An original reaction mechanism, entirely different from ordinary lithium–sulfur batteries<sup>[23,34]</sup> was demonstrated, where five fixed derivative peaks between 400 and 600 nm that represent the lithium sulfide and selenide products of Li<sub>2</sub>SSe, Li<sub>2</sub>S<sub>2</sub>Se, RSLi, RS<sub>2</sub>Li, and RS<sub>2</sub>SeLi. In addition, the responses of other reduction products of insoluble Li<sub>2</sub>S and Li<sub>2</sub>Se to UV/vis cannot be detected.<sup>[23,34]</sup> Therefore, a new reaction process has been confirmed where no long-chain soluble polysulfides are formed, enabling a stable cycling performance and high Coulombic efficiency. In order to investigate the following delithiation process, we also conducted in situ UV/vis spectroscopy at different stages during the charging process (Figure S11, Supporting Information). Apparently, during charging, no new derivative peaks representing long-chain polysulfide show up and no peak shifts (peaks would shift from short to long wavelengths if the long-chain polysulfides are produced during charging)<sup>[23,34]</sup> can be observed, which validates the production of long-chain lithium polysulfides is restricted.

In summary, to improve the volumetric/areal capacities and Coulombic efficiency, a new promising battery material of selenium-doped organic polymer (PDATtSSe) as a cathode material for lithium–organosulfur batteries was demonstrated. DFT calculations and in situ UV/vis spectroscopy reveal that no long-chain polysulfides were generated during cycling due to novel reaction chemistries resulting from the improvement of the molecular structure through selenium doping, leading to a ≈100% Coulombic efficiency and satisfactory cycling stability. The prepared electrodes exhibited a high gravimetric capacity of 700 mAh g<sup>-1</sup>, close to its theoretical mass capacity, an exceptional volumetric capacity of 2457 mAh cm<sup>-3</sup>, and a high areal capacity of 5.0 mAh cm<sup>-2</sup>. The superior electrochemical performance is due to the dense structure, and high electronic and ionic conductivity of the active materials, promoted through selenium doping, which are crucial parameters for the practical application of lithium–sulfur batteries.

## Supporting Information

Supporting Information is available from the Wiley Online Library or from the author.

## Acknowledgements

The authors acknowledge the support from the National Natural Science Foundation of China (No. 51402202, No. 51622208), China Postdoctoral

Science Foundation (No. 2015M570474, No. 2016T90491), and the Priority Academic Program Development of Jiangsu Higher Education Institutions (PAPD).

## Conflict of Interest

The authors declare no conflict of interest.

## Keywords

Coulombic efficiency, lithium–organosulfur batteries, Se doping, shuttle effect, volumetric capacity

Received: March 7, 2017

Revised: June 7, 2017

Published online: July 10, 2017

- [1] B. Kang, G. Ceder, *Nature* **2009**, *458*, 190.
- [2] Z. W. Seh, W. Y. Li, J. J. Cha, G. Y. Zheng, Y. Yang, M. T. McDowell, P. C. Hsu, Y. Cui, *Nat. Commun.* **2013**, *4*, 1331.
- [3] X. N. Li, J. W. Liang, K. L. Zhang, Z. G. Hou, W. Q. Zhang, Y. C. Zhu, Y. T. Qian, *Energy Environ. Sci.* **2015**, *8*, 3181.
- [4] P. G. Bruce, S. A. Freunberger, L. J. Hardwick, J. M. Tarascon, *Nat. Mater.* **2012**, *11*, 19.
- [5] L. Ma, H. L. Zhuang, S. Y. Wei, K. E. Hendrickson, M. S. Kim, G. Cohn, R. G. Hennig, L. A. Archer, *ACS Nano* **2016**, *10*, 1050.
- [6] A. Manthiram, S. H. Chung, C. X. Zu, *Adv. Mater.* **2015**, *27*, 1980.
- [7] Z. K. Zhang, J. H. Du, D. D. Zhang, H. D. Sun, L. C. Yin, L. P. Ma, J. S. Chen, D. G. Ma, H. M. Cheng, W. C. Ren, *Nat. Commun.* **2017**, *8*, 14560.
- [8] P. F. Hu, H. Wang, Y. Yang, J. Yang, J. Lin, L. Guo, *Adv. Mater.* **2016**, *28*, 3486.
- [9] S. W. Wang, L. J. Wang, K. Zhang, Z. Q. Zhu, Z. L. Tao, J. Chen, *Nano Lett.* **2013**, *13*, 4404.
- [10] Z. P. Song, Y. M. Qian, M. L. Gordin, D. H. Tang, T. Xu, M. Otani, H. Zhan, H. S. Zhou, D. H. Wang, *Angew. Chem. Int. Ed.* **2015**, *127*, 14153.
- [11] J. Tang, L. B. Kong, J. Y. Zhang, L. Z. Zhan, H. Zhan, Y. H. Zhou, C. M. Zhan, *React. Funct. Polym.* **2008**, *68*, 1408.
- [12] J. Gao, M. A. Lowe, S. Conte, S. E. Burkhardt, H. D. Abruça, *Chem. - Eur. J.* **2012**, *18*, 8521.
- [13] A. Manthiram, Y. Z. Fu, S. H. Chung, C. X. Zu, Y. S. Su, *Chem. Rev.* **2014**, *114*, 11751.
- [14] G. J. Hu, Z. H. Sun, C. Shi, R. P. Fang, J. Chen, P. X. Hou, C. Liu, H. M. Cheng, F. Li, *Adv. Mater.* **2017**, *29*, 1603835.
- [15] J. Ding, H. Zhou, H. L. Zhang, T. Stephenson, Z. Li, D. Karpuzov, D. Mitlin, *Energy Environ. Sci.* **2017**, *10*, 153.
- [16] H. L. Ye, L. Wang, S. Deng, X. Q. Zeng, K. Q. Nie, P. N. Duchesne, B. Wang, S. Liu, J. H. Zhou, F. P. Zhao, N. Han, P. Zhang, J. Zhong, X. H. Sun, Y. Y. Li, Y. G. Li, J. Lu, *Adv. Energy Mater.* **2017**, *7*, 1601602.
- [17] C. Luo, Y. H. Xu, Y. J. Zhu, Y. H. Liu, S. Y. Zheng, Y. Liu, A. Langrock, C. S. Wang, *ACS Nano* **2013**, *7*, 8003.
- [18] C. P. Yang, S. Xin, Y. X. Yin, H. Ye, J. Zhang, Y. G. Guo, *Angew. Chem. Int. Ed.* **2013**, *52*, 8363.
- [19] F. G. Sun, H. Y. Cheng, J. Z. Chen, N. Zheng, Y. S. Li, J. L. Shi, *ACS Nano* **2016**, *10*, 8289.
- [20] W. J. Chung, J. J. Griebel, E. T. Kim, H. Yoon, A. G. Simmonds, H. J. Ji, P. T. Dirlam, R. S. Glass, J. J. Wie, N. A. Nguyen, B. W. Guralnick, J. Park, A. Somogyi, P. Theato, M. E. Mackay, Y. E. Sung, K. Char, J. Pyun, *Nat. Chem.* **2013**, *5*, 518.

- [21] S. R. Chen, F. Dai, M. L. Gordin, Z. X. Yu, Y. Gao, J. X. Song, D. H. Wang, *Angew. Chem.* **2016**, *128*, 4303.
- [22] T. M. Johnson, *Chem. Geol.* **2004**, *204*, 201.
- [23] N. Xu, T. Qian, X. L. Liu, J. Liu, Y. Chen, C. L. Yan, *Nano Lett.* **2017**, *17*, 538.
- [24] C. Huang, J. Xiao, Y. Y. Shao, J. M. Zheng, W. D. Bennett, D. P. Lu, L. V. Saraf, M. Engelhard, L. W. Ji, J. G. Zhang, X. L. Li, G. L. Graff, J. Liu, *Nat. Commun.* **2014**, *5*, 3015.
- [25] H. J. Peng, J. Q. Huang, X. B. Cheng, Q. Zhang, *Adv. Energy Mater.* **2017**, <https://doi.org/10.1002/aenm.201700260>.
- [26] X. B. Cheng, H. J. Peng, J. Q. Huang, R. Zhang, C. Z. Zhao, Q. Zhang, *ACS Nano* **2015**, *9*, 6373.
- [27] L. Qie, A. Manthiram, *Adv. Mater.* **2015**, *27*, 1694.
- [28] X. Ji, S. Evers, R. Black, L. F. Nazar, *Nat. Commun.* **2011**, *2*, 325.
- [29] X. Yang, L. Zhang, F. Zhang, Y. Huang, Y. S. Chen, *ACS Nano* **2014**, *5*, 5208.
- [30] J. Q. Zhou, T. Qian, M. F. Wang, N. Xu, Q. Zhang, Q. Li, C. L. Yan, *ACS Appl. Mater. Interfaces* **2016**, *8*, 5358.
- [31] X. Y. Tao, Y. Y. Liu, W. Liu, G. M. Zhou, J. Zhao, D. C. Lin, C. X. Zu, O. W. Sheng, W. K. Zhang, H. W. Lee, Y. Cui, *Nano Lett.* **2017**, *17*, 2967.
- [32] H. Kim, J. Lee, H. Ahn, O. Kim, M. J. Park, *Nat. Commun.* **2015**, *6*, 7278.
- [33] D. P. Lv, J. M. Zheng, Q. Y. Li, X. Xie, S. Ferrara, Z. M. Nie, L. B. Mehdi, N. D. Browning, J. G. Zhang, G. L. Graff, J. Liu, J. Xiao, *Adv. Energy Mater.* **2015**, *5*, 1402290.
- [34] M. U. M. Patel, R. Dominko, *ChemSusChem* **2014**, *7*, 2167.